Title

Efficient Specification of Interneurons from Human Pluripotent Stem Cells by Dorsoventral and Rostrocaudal Modulation

Journal

Stem Cells, 32(7)

ISSN

1066-5099

Authors

Kim, Tae-Gon
Yao, Ruiqin
Monnell, Travis
et al.

Publication Date

2014-07-01

DOI

10.1002/stem.1704

Peer reviewed

STEM CELLS®

EMBRYONIC STEM CELLS/INDUCED PLURIPOTENT STEM CELLS

Efficient Specification of Interneurons from Human Pluripotent Stem Cells by Dorsoventral and Rostrocaudal Modulation

TAE–GON KIM,[a,b] RUIQIN YAO,[a,b] TRAVIS MONNELL,[a,b] JUN–HYEONG CHO,[c] ANJU VASUDEVAN,[d] ALICE KOH,[a,b] PEEYUSH KUMAR T.,[d] MINHO MOON,[a,b] DEBKANYA DATTA,[a,b] VADIM Y. BOLSHAKOV,[c] KWANG–SOO KIM,[a,b] SANGMI CHUNG[a,b]

Key Words. Pluripotent stem cells • Medial ganglionic eminence • Interneurons • Differentiation

[a]Molecular Neurobiology Laboratory, Department of Psychiatry and Program in Neuroscience, [b]Harvard Stem Cell Institute, [c]Cellular Neurobiology Laboratory, Department of Psychiatry, and [d]Angiogenesis & Brain Development Laboratory, Department of Psychiatry, McLean Hospital/Harvard Medical School, Belmont, Massachusetts, USA

Correspondence: Kwang-Soo Kim, Ph.D., McLean Hospital/Harvard Medical School, 115 Mill Street, Belmont, Massachusetts 02178, USA. Telephone: 617-855-2024; Fax: 617-855-3479; e-mail: kskim@mclean.harvard.edu; or Sangmi Chung, Ph.D., McLean Hospital/Harvard Medical School, 115 Mill Street, Belmont, Massachusetts 02178, USA. Telephone: 617-855-3478; Fax: 617-855-2020; e-mail: schung@mclean.harvard.edu.

Received July 4, 2013; ; first published online in STEM CELLS *EXPRESS* March 19, 2014.

1066-5099/2014/$30.00/0

http://dx.doi.org/10.1002/stem.1704

ABSTRACT

GABAergic interneurons regulate cortical neural networks by providing inhibitory inputs, and their malfunction, resulting in failure to intricately regulate neural circuit balance, is implicated in brain diseases such as Schizophrenia, Autism, and Epilepsy. During early development, GABAergic interneuron progenitors arise from the ventral telencephalic area such as medial ganglionic eminence (MGE) and caudal ganglionic eminence (CGE) by the actions of secreted signaling molecules from nearby organizers, and migrate to their target sites where they form local synaptic connections. In this study, using combinatorial and temporal modulation of developmentally relevant dorsoventral and rostrocaudal signaling pathways (SHH, Wnt, and FGF8), we efficiently generated MGE cells from multiple human pluripotent stem cells. Most importantly, modulation of FGF8/FGF19 signaling efficiently directed MGE versus CGE differentiation. Human MGE cells spontaneously differentiated into Lhx6-expressing GABAergic interneurons and showed migratory properties. These human MGE-derived neurons generated GABA, fired action potentials, and displayed robust GABAergic postsynaptic activity. Transplantation into rodent brains results in well-contained neural grafts enriched with GABAergic interneurons that migrate in the host and mature to express somatostatin or parvalbumin. Thus, we propose that signaling modulation recapitulating normal developmental patterns efficiently generate human GABAergic interneurons. This strategy represents a novel tool in regenerative medicine, developmental studies, disease modeling, bioassay, and drug screening. STEM CELLS *2014;32:1789–1804*

INTRODUCTION

During early development, cortical interneuron progenitors arise from the ventral telencephalic area such as medial ganglionic eminence (MGE) and caudal ganglionic eminence (CGE) [1]. Among these, MGE progenitors mostly generate Parvalbumin-expressing interneurons or Somatostatin-expressing interneurons comprising approximately 65% of the entire cortical interneuron population, whereas CGE cells mostly generate Calretinin-expressing interneurons [2]. Combined and temporal actions of secreted signaling molecules from nearby organizers play a crucial role during this early phenotype specification of ventral telencephalon, such as Sonic Hedge Hog SHH [3, 4], Wnt [5], and Fibroblast Growth Factor 8 (FGF8) [6, 7]. These initial extrinsic signals initiate the regulatory cascades leading to cortical interneuron development by inducing key transcription factors such as Nkx2.1 in MGE progenitors [8], followed by Lhx6 in postmitotic interneurons [9]. Originating ventrally, MGE-derived GABAergic interneurons migrate to their target sites where they form local synaptic connections with glutamatergic projection neurons and critically modulate cortical circuitry.

Dysfunction of interneurons has been implicated in various brain diseases such as Epilepsy, Schizophrenia, and Autism [10], conditions awaiting more effective treatments. Human pluripotent stem cell (hPSC) technology provides an unprecedented opportunity to study disease mechanisms and develop novel therapeutics for these brain disorders [11–16]. Recent reports on the generation of interneurons from hPSCs [17–19] commonly use ventralizing SHH activation but with conflicting results on timing of activation. Whereas Nicholas et al. observed that early activation of SHH (starting day 0) results in approximately 75% MGE phenotype induction ($Nkx2.1^+Olig2^+$), Maroof et al. showed that early activation of SHH generates >80% $Nkx2.1^+Olig2^-FoxG1^-$ ventral diencephalic progenitors and only late SHH activation (starting day 10) generated MGE cells ($Nkx2.1^+Olig2^+$) albeit less efficiently

(approximately 50%). Such discrepancy requires further optimization of MGE derivation from hPSCs for their efficient applications.

Here, we show that SHH activation during early human neural development elicits a pleiotropic downstream cascade, by inducing rostralizing FGF8 signaling as well as caudalizing FGF15/19 signaling, as observed during early mouse development [6, 20–24]. Such dual effect of SHH on rostral-caudal boundary determination can cause MGE derivation stochasticity depending on the fine balance of its downstream cascade. Thus, by combining early activation of SHH with exogenous rostralizing factor FGF8, we reliably induced MGE cells using early and strong SHH activation (>80% by fluorescence-activated cell sorting [FACS]) from multiple hPSCs. These cells shared characteristics with their in vivo counterpart, such as spontaneous differentiation into Lhx6-expressing and migrating GABAergic interneurons that can generate GABA, fire action potentials, and form functional GABAergic synaptic connections. Transplantation of human MGE cells into rodent brains yields well-contained neural grafts enriched with GABAergic interneurons that migrate in the host brain and mature to express somatostatin or parvalbumin.

Materials and Methods

PSC Culture and Differentiation

Human PSC cells H9 embryonic stem cells (ESCs) (WA09, WiCell, Madison, WI, (http://www.wicell.org) passages 45–55), H7 ESC (WA07, WiCell, passages 41–51), and iPSC2497 (a kind gift from Dr. Fred Gage [14], passages 30–40) were maintained on Matrigel (BD, San Jose, CA (http://www.bdbiosciences.com)) in mTeSR media (Invitrogen, Carlsbad, CA (http://www.lifetechnologies.com/us/en/home.html)) with 10 ng/ml bFGF (Peprotech, Rocky Hill, NJ (http://www.peprotech.com)), and passaged using Dispase (Stem Cell Technologies, Vancouver, BC, Canada (http://www.stemcell.com)). For differentiation, PSCs were trypsinized and grown as floating aggregates in low adherent flasks in Knockout Serum Replacement (KSR) media (20% knockout serum replacement, Dulbecco's modified Eagle's medium, 2mM L-glutamine, and 10 μM β-mercaptoethanol [all from Invitrogen, Carlsbad, CA (http://www.lifetechnologies.com/)]). Rock inhibitor (Y-27632, 10 μM, Tocris, Bristol, U.K. (http://www.tocris.com)) was added on the first day of differentiation. After 2 weeks of floating culture, cells were transferred to polyornithine (PLO; 15 mg/ml; Sigma, St. Louis, MO (http://www.sigmaaldrich.com)) and fibronectin (FN; 1 mg/ml; Sigma, St. Louis, MO (http://www.sigmaaldrich.com))-coated surfaces. For neural induction, cells were treated with LDN193189 (100 nM, Stemgent, Cambridge, MA (www.stemgent.com)) from day 0 to day 14 and with SB431542 (10 μM, Tocris, Bristol, U.K. (http://www.tocris.com)) from day 0 to day 7 [25]. For MGE induction, cells were treated with IWP2 (5 μM, EMD Millipore, Billerica, MA (http://www.emdmillipore.com/)) from day 0 to day 7, with Smoothened Agonist (SAG) (0.1 μM, EMD Millipore, Billerica, MA (http://www.emdmillipore.com)) from day 0 to day 21, and with FGF8 (100 ng/ml, Peprotech, Rocky Hill, NJ (http://www.peprotech.com)) from day 8 to day 21. After 3 weeks of differentiation, cells were trypsinized and droplets of 10,000 cells per microliter transferred to PLO/FN-coated coverslips in differentiation media (N3 media [26] with 10 ng/ml Glial cell line-derived neurotrophic factor (GDNF) [Peprotech, Rocky Hill, NJ (http://www.peprotech.com)], 10 ng/ml Brain-derived neurotrophic factor (BDNF) [Peprotech, Rocky Hill, NJ (http://www.peprotech.com)], and 2.5 μM gamma secretase inhibitor, DAPT [Tocris, Bristol, U.K. (http://www.tocris.com)]) for further differentiation and maturation.

For Matrigel two-dimensional migration analysis, MGE cells or control cells (Pax6+ cells without IWP2, SAG, and FGF8 treatment) were trypsinized at day 21 of differentiation and reaggregated in low attachment round-bottomed 96-well plate in differentiation media (10,000 cells/well). MGE spheres or cortical spheres were plated on coverslips coated with 1:100 diluted Matrigel in differentiation media after 25 days of further differentiation and analyzed 5 days after plating. For analysis of migrating cell numbers, total cell numbers that migrated out of the spheres were counted, and then the cells were trypsinized to count the total cell numbers for normalization. For measuring migration distances, ImageJ software was used to assess each cell migration distance between the edge of the sphere and the center of the migrating cell body. Some of the spheres were also fixed for immunocytochemistry analysis.

For Matrigel two-dimensional migration analysis of mouse explant, E13.5 embryos were removed one at a time from anesthetized CD1 dams, brains were isolated, embedded in 8% low gelling temperature agarose (Sigma, St. Louis, MO (http://www.sigmaaldrich.com)), and cut at a thickness of 300 μm on a vibratome in the coronal plane. Both cortical and MGE regions were punched out from these coronal sections using a micropunch (Guide wire and tube assembly, 19 gauge; Inner Diameter 0.027 in., Small Parts, Inc., Miami Lakes, FL (http://www.smallpartsinc.com)) and collected in Neurobasal medium. E13.5 cortex or MGE explants were plated on coverslips coated with1:100 diluted Matrigel, and analyzed the same way as the human spheres. For Matrigel three-dimensional (3D) migration analysis, MGE explants or human MGE spheres were embedded in undiluted 3D matrigel matrix, cultured in differentiation media, and their migration was analyzed 2 days after embedding.

Slice Transplantation Analysis

E13.5 embryos were collected by hysterotomy of deeply anesthetized CD1 dams (Ketamine, 50 mg/kg and Xylazine, 10 mg/kg; i.p.) and decapitated immediately. Embryonic brains were isolated and embedded in 8% low gelling temperature agarose (Sigma, St. Louis, MO (http://www.sigmaaldrich.com)). Coronal slices (250–300-μm thick) of telencephalon were prepared and transferred to polycarbonate membrane filters (Invitrogen, Carlsbad, CA (http://www.lifetechnologies.com)) in sterile six-well plates containing Neurobasal medium (Invitrogen, Carlsbad, CA (http://www.lifetechnologies.com)). Control spheres and MGE spheres, that were prepared as described above and prelabeled with QDot 655 nanocrystals (Invitrogen, Carlsbad, CA (http://www.lifetechnologies.com)) according to the manufacturer's instructions (cells incubated in 10 nM labeling solution at 37°C for an hour), were inserted using fine tungsten needles into the ventral telencephalon of CD1 slices under a high power stereomicroscope. Slices were cultured for 48 hours, fixed in zinc fixative (BD Pharmingen, Franklin Lakes, NJ (http://www.bd.com)) and processed for paraffin wax histology. Neural cell adhesion molecule (NCAM) immunohistochemistry was performed on 20-μm-thick paraffin sections with a mouse monoclonal anti-NCAM antibody raised against CD56-positive

Table 1. Antibody list used in the experiments

Antibody	Species	Dilution	Source
β-tubulin	Rabbit	1/2,000	Covance
β-tubulin	Mouse	1/2,000	Covance
Calbindin	Rabbit	1/10,000	Swant
Calretinin	Goat	1/5,000	Swant
CoupTFII	Mouse	1/1,000	Persus Proteomics
FoxG1	Rabbit	1/500	Abcam
GABA	Rabbit	1/1,000	Sigma
GAD 65/67	Rabbit	1/1,000	Millipore
Glutamate	Rabbit	1/15000	Sigma
Isl1	Mouse	1/1,000	DSHB
Lhx6	Rabbit	1/1,000	Gift from Dr. Pachnis
NCAM	Mouse	1/1,000	SCBT
Nestin	Mouse	1/1,000	Millipore
Neuropeptide Y	Sheep	1/5,000	Millipore
Nkx2.1 (TTF1)	Rabbit	1/2,000	Epitomics
Human Nucleus	Mouse	1/1,000	Millipore
0lig2	Rabbit	1/500	Millipore
Parvalbumin	Mouse	1/5,000	Millipore
Pax6	Rabbit	1/200	Covance
Pax6	Mouse	1/1,000	DSHB
PSD-95	Rabbit	1/1,000	Cell Signaling
PSD-95	Mouse	1/1,000	Neuro Mab
Somatostatin	Rat	1/5,000	Millipore
Synaptophysin	Rabbit	1/2,000	Pierce
Synaptophysin	Mouse	1/500	Abcam
VGLUT	Mouse	1/1,000	DSHB
NeuN	Mouse	1/500	Chemicon
VGAT	Rabbit	1/1,000	Synaptic Systems
Gephyrin	Mouse	1/1,000	Synaptic Systems
Human Cytoplasm	Mouse	1/500	Stem Cells Inc
NKX2.2	Mouse	1/1,000	DSHB
SP8	Goat	1/500	SBT
ER81	Goat	1/1,000	SCBT
Tbr1	Rabit	1/500	Abeam
ChAT	Goat	1/500	Millipore
DARPP32	Rabbit	1/500	SCBT
VIP	Rabbit	1/1,000	Immunostar, Inc.
Pitx3	Rabbit	1/1,000	Gift from Dr. Burbach
TH	Sheep	1/1,000	Pelfreez
Ki67	Mouse	1/1,000	Millipore
Sox6	Rabbit	1/1,000	Millipore
Somatostatin	Goat	1/1,000	SCBT
CNPase	Mouse	1/1,000	Sigma
GFAP	Rabbit	1/1,000	Dako

cells of human origin (Santa Cruz, Dallas, TX (http://www.scbt.com)) and mounted with DAPI (Vector Laboratories, Burlingame, CA (https://www.vectorlabs.com)). Other antibodies used were mouse anti-human cytoplasm antibody (Stem Cell, Inc., Vancouver, BC, Canada (http://www.stemcell.com)) and cy3-conjugated anti-human nuclei antibody (Millipore, Billerica, MA (http://www.millipore.com)). Images were captured from an FSX100 microscope (Olympus, Center Valley, PA (http://www.olympusamerica.com)). The number of $NCAM^+$ cells that migrated from ventral to dorsal telencephalon in the three panels depicted in the schema was determined by ImageJ software and average values obtained. Statistical significance of differences between groups was analyzed by two-tailed Student's *t* test (Prism6; GraphPad software). Results were expressed as mean $\pm$ SD and statistical significance was reported at $p < .05$.

FACS Analysis

Differentiated cells were trypsinized and fixed in Fix/Perm solution (BD, Franklin Lakes, NJ (http://www.bdbiosciences.com)) for 30 minutes, and incubated with blocking buffer (Phosphate buffered saline (PBS) with 0.1 mg/ml Bovine serum albumin (BSA) and 0.1% Saponin [both from Sigma, St. Louis, MO (http://www.sigmaaldrich.com)]) for 10 minutes. Blocked cells were incubated with primary antibody (anti-Nkx2.1; Epitomics, Burlingame, CA (http://www.epitomics.com)) in blocking buffer for 30 minutes. After washing with PBS, Alexa 647-conjugated secondary antibodies (Invitrogen, Carlsbad, CA (http://www.lifetechnologies.com)) were added (1:1,000) and incubated for another 15 minutes. Some samples were incubated only with secondary antibody as control. After washing with PBS, cells were suspended in blocking buffer and analyzed using a FACSAria (BD Biosciences, San Jose, CA (http://www.bdbiosciences.com)). Flowjo (Tree Star, Ashland, Or (http://www.treestar.com)) software was used to analyze raw data. 10,000 cells were used per analysis.

Real-Time PCR Analysis

Total RNA was prepared using Trizol (Invitrogen, Carlsbad, CA (http://www.lifetechnologies.com)) and Purelink RNA mini kit (Invitrogen, Carlsbad, CA (http://www.lifetechnologies.com)). cDNA from total RNA was generated using the SuperScript II RT (Invitrogen, Carlsbad, CA (http://www.lifetechnologies.com)) and oligo (dT) primers. For quantitative analysis of the expression level of mRNAs, real-time PCR analyses were performed using the DNA engine Opticon (MJ Research, Waltham, MA (www.bio-rad.com)) and SYBR green I (Molecular Probes, Eugene, OR (http://www.lifetechnologies.com)). Primers were designed using the MacVector software (Oxford Molecular, Ltd.: primers sequences are available upon request). PCR was performed in 25 μl containing 0.5 mM of each primer, 0.5× SYBR Green I (Molecular Probes, Eugene, OR (http://www.lifetechnologies.com)), and 1 μl of cDNA. Fifty cycles consisting of 95°C for 30 seconds, 55°C for 30 seconds, 72°C for 30 seconds, and 79°C for 5 seconds were performed. Primer dimers were melted at 79°C before measuring the fluorescent signals after each cycle. The mRNA expression level for each gene was normalized against that of the GAPDH gene. The relative values were calculated by setting the normalized value of control as 1.

Immunocytochemistry and Immunohistochemistry

For immunofluorescence staining, fixed cells or tissue sections were incubated with blocking buffer (PBS, 10% normal donkey serum [NDS]) containing 0.1% Triton for 10 minutes. Cells were then incubated overnight at 4°C with primary antibodies diluted in PBS containing 2% NDS. The primary antibody list can be found in Table 1. After rinsing with PBS, samples were incubated with fluorescent dye-labeled secondary antibodies (Alexa 488-, Alexa 594-, or Alexa 647-labeled IgG; Invitrogen, Carlsbad, CA (http://www.lifetechnologies.com)) in PBS containing 2% NDS for 30 minutes at room temperature. After rinsing with PBS, Hoechst 33342 (4 mg/ml) was used for counterstaining, and coverslips/tissues sections were mounted onto slides in Mowiol 4–88 (Calbiochem, Gibbstown, NJ (www.emdmillipore.com)). Confocal analysis was performed using an Olympus DSU Spinning Disc Confocal on an IX81 inverted microscope (Olympus Center Valley, PA).

Cell Counting and Statistical Analysis

Cells were counted using the StereoInvestigator image capture equipment and software (MicroBrightField, Williston, VT). For

counting of cells on coverslips, an optical fractionator probe was used with a 500 μm × 500 μm grid size and 100 μm × 100 mm counting frame (>40 counting sites with >1,000 total cells counted per sample) at ×40 magnification. Coverslips from three to four independent differentiations were used for analysis. For statistical analysis, we performed *t* test (alpha = 0.05) comparing control versus sample using Prism6 software (Graph Pad).

HPLC Assay

Cellular GABA content was measured by High-performance liquid chromatography (HPLC) from MGE cells and cortical cells as control after 60 days of differentiation, as described previously [26]. Cells were homogenized, using a tissue dismembrator, in 100–750 μl of 0.1 M TCA supplemented with 10^{-2} M sodium acetate, 10^{-4} M Ethylenediaminetetraacetic acid (EDTA), 5 ng/ml isoproterenol (as internal standard), and 10.5% methanol (pH 3.8). Samples were spun in a microcentrifuge at 10,000*g* for 20 minutes. Supernatants were collected and analyzed by HPLC while protein determination was performed on the pellets for normalization of the HPLC data. Amino acids were determined by the Waters AccQ-Tag system using a Waters 474 Scanning Fluorescence Detector. The Empower 2 software was used to control the HPLC gradient profile and data acquisition.

Electrophysiological Analysis

MGE cells were differentiated for 6 or 12 weeks in differentiation media and transferred into a recording chamber that was continuously perfused with artificial cerebrospinal fluid containing 130 mM NaCl, 2.5 mM KCl, 2.5 mM $CaCl_2$, 1 mM $MgSO_4$, 1.25 mM NaH_2PO_4, 26 mM $NaHCO_3$, and 10 mM glucose with 95% O_2 and 5% CO_2 at a rate of 1 ml per minute at room temperature (21°C–23°C). Whole-cell patch-clamp recordings were performed at 24°C–25°C using an EPC-9 amplifier and Pulse v8.8 software (HEKA Elektronik). The patch electrodes (2–3 MΩ resistance) were filled with a solution of 140 mM KCl, 5 mM NaCl, 1 mM $MgCl_2$, 10 mM HEPES, 0.2 mM ethylene glycol tetraacetic acid (EGTA), 2 mM Mg ATP, and 0.5 mM Na GTP (285 mOsm, adjusted to pH 7.3 with KOH). Liquid junction potential of 3.1 mV was not corrected. Series resistance was compensated at 50%–60%. Offline data analysis was performed using the Clampfit 9 program (Molecular Devices). Reagents were purchased from Tocris Bioscience (Bristol, U.K. (http://www.tocris.com)) (tetrodotoxin) or Sigma-Aldrich (St. Louis, MO (http://www.sigmaaldrich.com)) (bicuculline methochloride).

Transplantation Analyses

The Animal Care and Use Committee at McLean Hospital approved all animal procedures. H9-derived MGE cells at 5 weeks of differentiation were trypsinized and suspended to a final concentration of 50,000 cells per microliter in transplantation media (Hank's balanced salt solution (HBSS) with 10 ng/ml GDNF, 10 ng/ml BDNF, and 20 μM Boc-Asp(OMe) fluoromethyl ketone [Sigma-Aldrich, St. Louis, MO (http://www.sigmaaldrich.com)]). One microliter was injected into each striatum of NOD SCID mice (from the bregma: AP +0.05, L ±0.18, V −0.30, IB 9) using a 22-gauge, 5 ml Hamilton syringe, and a Kopf stereotaxic frame (Kopf Instruments, Tujunga, CA (http://www.kopfinstruments.com)). Cortically induced cells without signaling pathway activation were also transplanted as control ($n = 10$). Before surgery, mice received an i.p. injection of acepromazine (3.3 mg/kg, PromAce, Fort Dodge, IA) and atropine sulfate (0.2 mg/kg, Phoenix Pharmaceuticals, St. Joseph, MO) followed by anesthesia with an i.p. injection of ketamine (60 mg/kg, Fort Dodge) and xylazine (3 mg/kg, Phoenix Pharmaceuticals). Transplanted mice were terminally anesthetized with an i.p. overdose of pentobarbital (150 mg/kg, Sigma) and perfused intracardially with heparin saline (0.1% heparin in saline) followed by formaldehyde (4%) 5 weeks or 5 months postgrafting. Brains were removed, postfixed in 4% formaldehyde, equilibrated in 20% sucrose, and 40-mm coronal slices obtained using a freezing microtome. The StereoInvestigator image-capture equipment and software (MicroBrightField) were used for cell counting and estimation of total cell number in the graft using the serial section manager tool from every sixth sections. Total graft volume was also measured using the StereoInvestigator with the Cavalieri estimator probe and serial section manager tool from every sixth sections.

Results

MGE Cell Specification from hPSCs Recapitulates In Vivo Signaling Pathways

During early development, signaling molecules from organizers direct early neuroectoderm phenotype specification. Thus, to optimize the phenotype specification of MGE cells from hPSCs, we sought to understand temporal and combinatorial regulations by relevant signaling molecules. H9 cells were differentiated as floating spheres in the presence of LDN193189 and SB431542 to facilitate differentiation into neuroectodermal lineages of hPSCs [25]. Inhibition of Wnt signaling was shown to induce telencephalic identity during neural plate formation [27, 28], and thus, we used IWP2, a chemical inhibitor of Wnt signaling, to enhance rostralization of early neuroectoderm and subsequently to inhibit dorsalization of neuroectoderm [29]. We first tested the dosage of SHH signaling on phenotype specification of early neuroectoderm, since the degree of SHH activation regulates the subregional identity of Lateral Ganglionic Eminence (LGE) versus MGE within the ventral telencephalon [23]. At 10 nM SAG (Smoothened agonist), there was modest increase in MGE specification, but at 100 nM SAG, there was significantly higher induction of the MGE phenotype (Fig. 1A–1C, 1G). However, when we analyzed the expression of isl1, a general ventral telencephalic marker that is expressed in both MGE- and LGE-derived cells, there was no significant difference between 10 nM and 100 nM SAG (Fig. 1D–1F), suggesting that with high SHH activation, the number of MGE cells increased at the expense of LGE cells. Thus, we used 100 nM SAG for subsequent MGE induction experiments.

We next tested the optimal treatment time frame of each signaling molecules. Since we observed most of the cells express Pax6 by day 7 of differentiation (Supporting Information Fig. S1A–S1F), we tested whether modulation of Wnt and SHH signaling is optimal during or after neuroectoderm formation. With treatment starting at day 0 of differentiation, there was a significant increase in MGE specification compared to treatment starting at day 7 (Fig. 1H; IWP + SAG 6.77% vs. 24%), suggesting that regionalization signaling

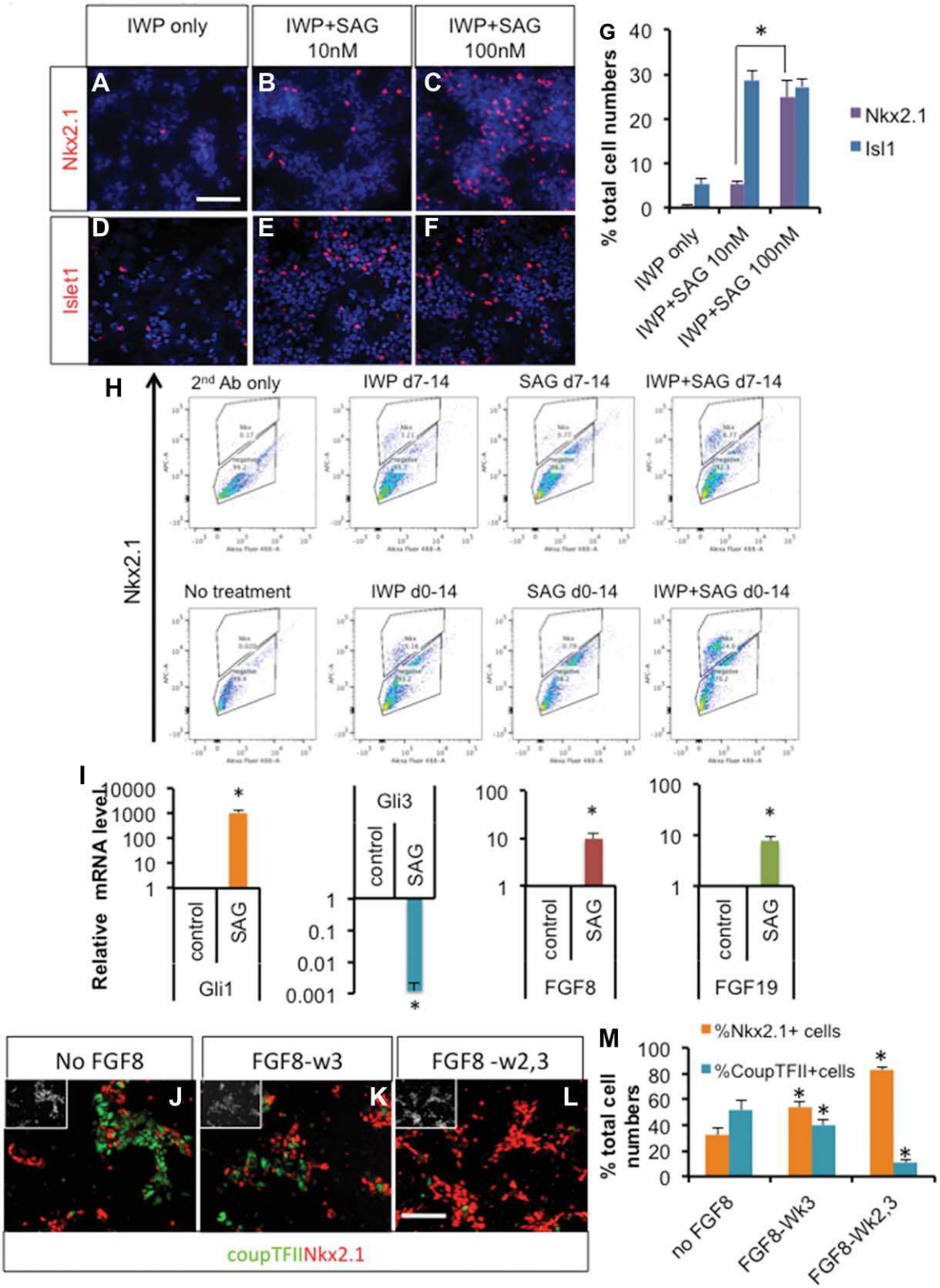

Figure 1. Directed differentiation of human pluripotent stem cells into ventral telencephalic phenotype. **(A–G):** Strong SHH signaling directs differentiating human H9 cells into medial ganglionic eminence (MGE) phenotype, assayed by immunocytochemistry and cell counting after 25 days of differentiation (mean ± SEM; $n = 4$, $p < .05$, two-tailed t test). **(H):** Optimization of MGE derivation from H9 cells by various combinations and timing of signaling activation, assayed by flow cytometry analysis after 25 days of differentiation. **(I):** Real-time PCR analysis of differentiating embryonic stem cells with or without 3 days' treatment with SAG (mean ± SEM; $n = 4$, $p < .05$, two-tailed t test). **(J–M):** FGF8 signaling further induced MGE phenotype at the expense of the caudal ganglionic eminence phenotype as shown by immunocytochemistry and cell counting analysis (mean ± SEM; $n = 3$, $p < .05$, two-tailed t test). White scale bar = 100 μm.

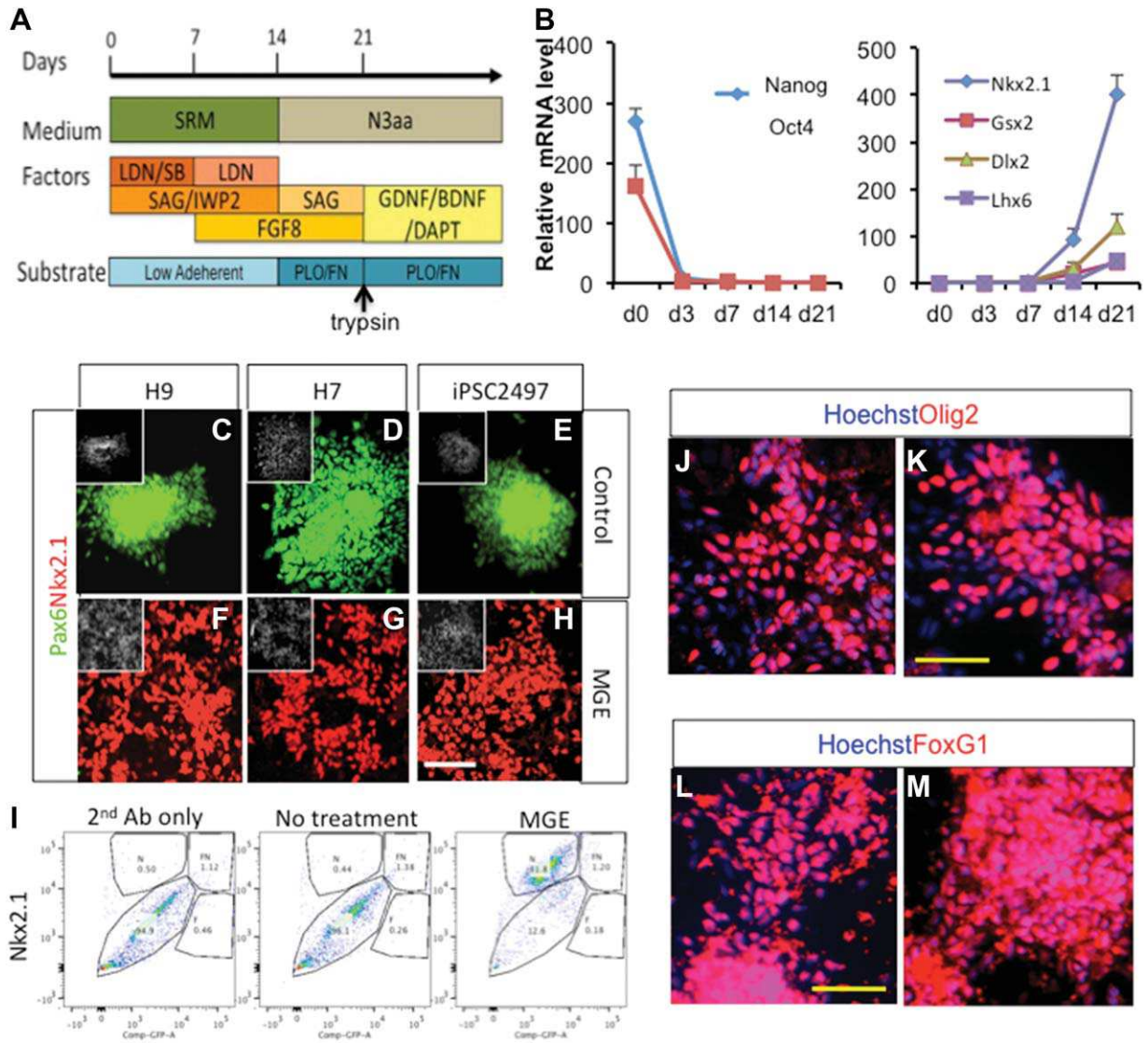

Figure 2. Optimized MGE derivation protocol efficiently generates MGE cells from multiple PSC lines. **(A):** Overview of optimized MGE derivation protocols. **(B):** Gene expression analysis during MGE derivation of H9 cells, assayed by real-time PCR (mean ± SEM; $n = 3$). **(C–H):** Combined and temporal treatment with IWP2, SAG, and FGF8 results in robust induction of MGE cells from H9 and H7 human embryonic stem cells as well as iPSC2497, assayed after 25 days of differentiation. White scale bar = 100 μm. **(I):** Fluorescence-activated cell sorting analysis of MGE generation of H9 cells after Nkx2.1 staining. **(J–M):** Derived cells highly express independent ventral telencephalic marker Olig2 and telencephalic marker FoxG1, assayed after 25 days of differentiation. Yellow scale bar = 50 μm. Abbreviations: iPSC, induced pluripotent stem cell; MGE, medial ganglionic eminence.

during early differentiation is more efficient than after neuroectoderm formation. Differentiating hPSCs were also treated with IWP2 or SHH alone or in combination. With single molecule treatment, there was only a mild increase in MGE specification, but the combination of Wnt blocker and SHH activator yielded a synergistic increase in MGE specification (Fig. 1H; 5.16% or 0.79% vs. 24%; with a day 0 start day). We observed similar results with Nkx2.1 mRNA expression levels by real-time PCR (Supporting Information Fig. 1G). Since SHH continues to be required for Nkx2.1 expression, even after initial specification of ventral telencephalic identity [30], we tested whether additional treatment with SHH is beneficial for MGE induction. As shown in Supporting Information Figure S1H, SAG treatment in the third week of differentiation increased Nkx2.1 level mildly but significantly.

Conflicting results from recent studies on early activation of the SHH pathway [17, 18] prompted us to investigate the downstream events triggered by SHH activation during early differentiation. As expected from previous studies [31, 32], there was strong induction of Gli1 activator by SHH activation as well as strong Gli3 expression reduction (Fig. 1I). Repression of Gli3 is accompanied by induction of the rostralizing signal FGF8 [6, 31], but at the same time, early SHH activation also induced the expression of FGF15/19 (Fig. 1I), which antagonizes the rostralizing effect of FGF8 during mouse telencephalic development [22, 24]. Thus, to compensate the effect of FGF15/19 induction by strong SHH activation, we tested the effect of exogenous addition of FGF8, to shift the balance toward rostralization. In the absence of FGF8 signaling, both MGE and CGE phenotypes appear, as shown by

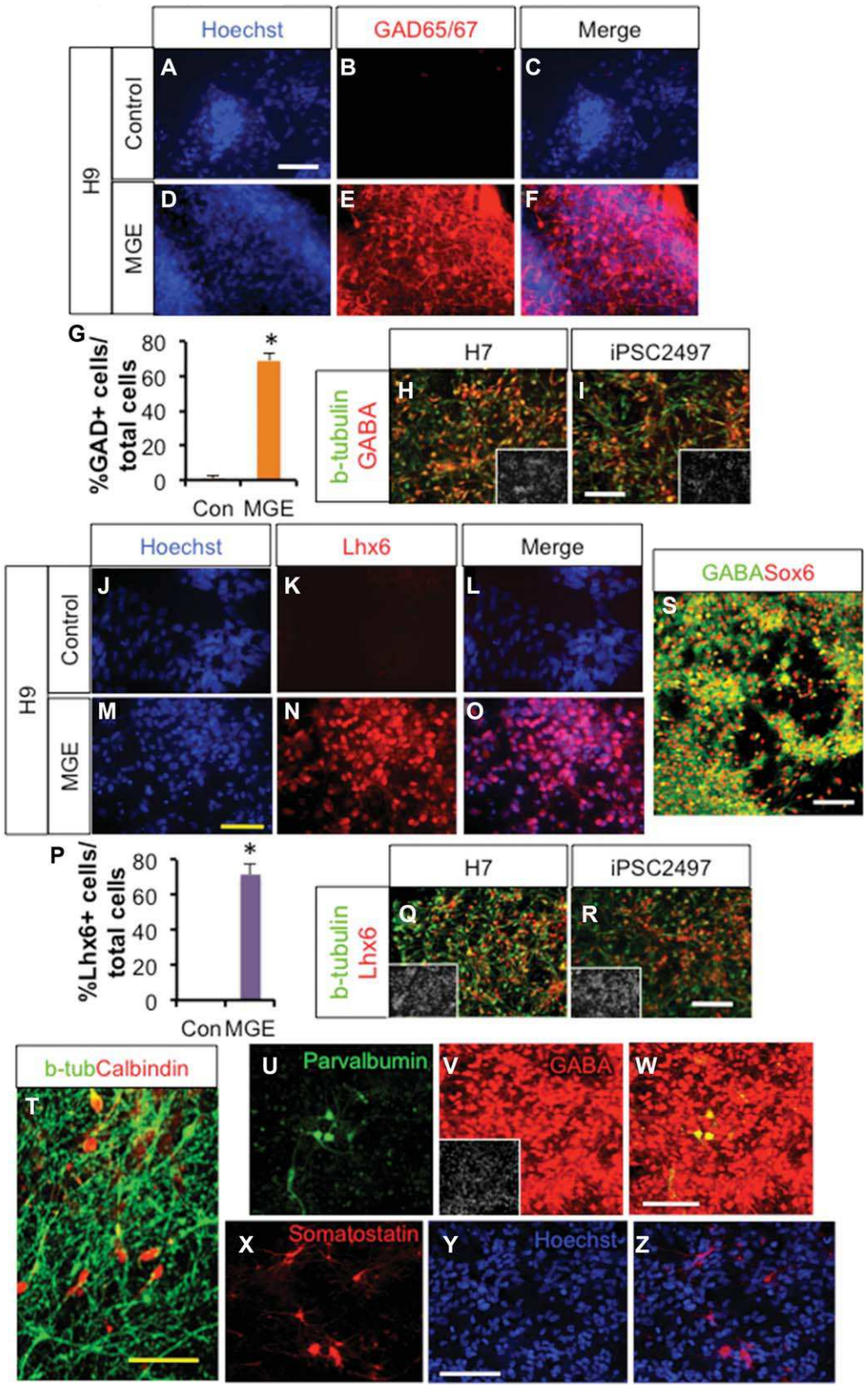

Figure 3. Human MGE cells generate GABAergic interneurons. **(A–G):** Combined and temporal treatments with IWP2, SAG, and FGF8 generate mostly GABAergic neurons from differentiating H9 cells, whereas in the absence of such treatment, few cells become GABAergic neurons. Immunocytochemistry and cell counting analysis after 6 weeks of differentiation (mean ± SEM; $n = 4$, $p < .05$, two-tailed t test). **(H, I):** H7 and iPSC2497-derived MGE cells also generate GABAergic neuron-enriched cultures. **(J–R):** Human PSC-derived MGE cells generate Lhx6+ neurons (mean ± SEM; $n = 4$, $p < .05$, two-tailed t test). **(S):** Human PSC-derived MGE cells generate Sox6+ GABAergic neurons. **(T–Z):** Some MGE-derived cells express Calbindin, Parvalbumin, or Somatostatin. White scale bar = 100 μm. Yellow scale bar = 50 μm. Abbreviations: iPSC, induced pluripotent stem cell; MGE, medial ganglionic eminence.

Nkx2.1 expression and CoupTFII expression (Fig. 1J–1M). FGF treatment in the second and/or third week of differentiation significantly increased MGE differentiation at the expense of CGE differentiation (Fig. 1J–1M), successfully counteracting SHH-induced caudalizing effect of FGF15/19. Furthermore, applying FGF19 exogenously instead of FGF8 resulted in most of the cells taking up CGE identity (Supporting Information Fig. S2A–S2E), further supporting the role of FGF8/FGF19 signaling in determining rostral/caudal telencephalic identity. Exogenous addition of FGF19 increased diencephalic differentiation as shown by Nkx2.2 expression (Supporting Information Fig. S2F, S2G; $0.61\% \pm 0.38\%$ Nkx2.2$^+$/total cells vs. $4.19\% \pm 0.77\%$ Nkx2.2$^+$/total cells for FGF8-treated and FGF19-treated cells, respectively, $n = 4$), but diencephalic cells remained a minority even with FGF19 treatment, suggesting that employment of early Wnt inhibitor successfully rostralized the early neuroectoderm to telencephalic identity. Since it has been reported that FGF8 can induce FGF19 expression

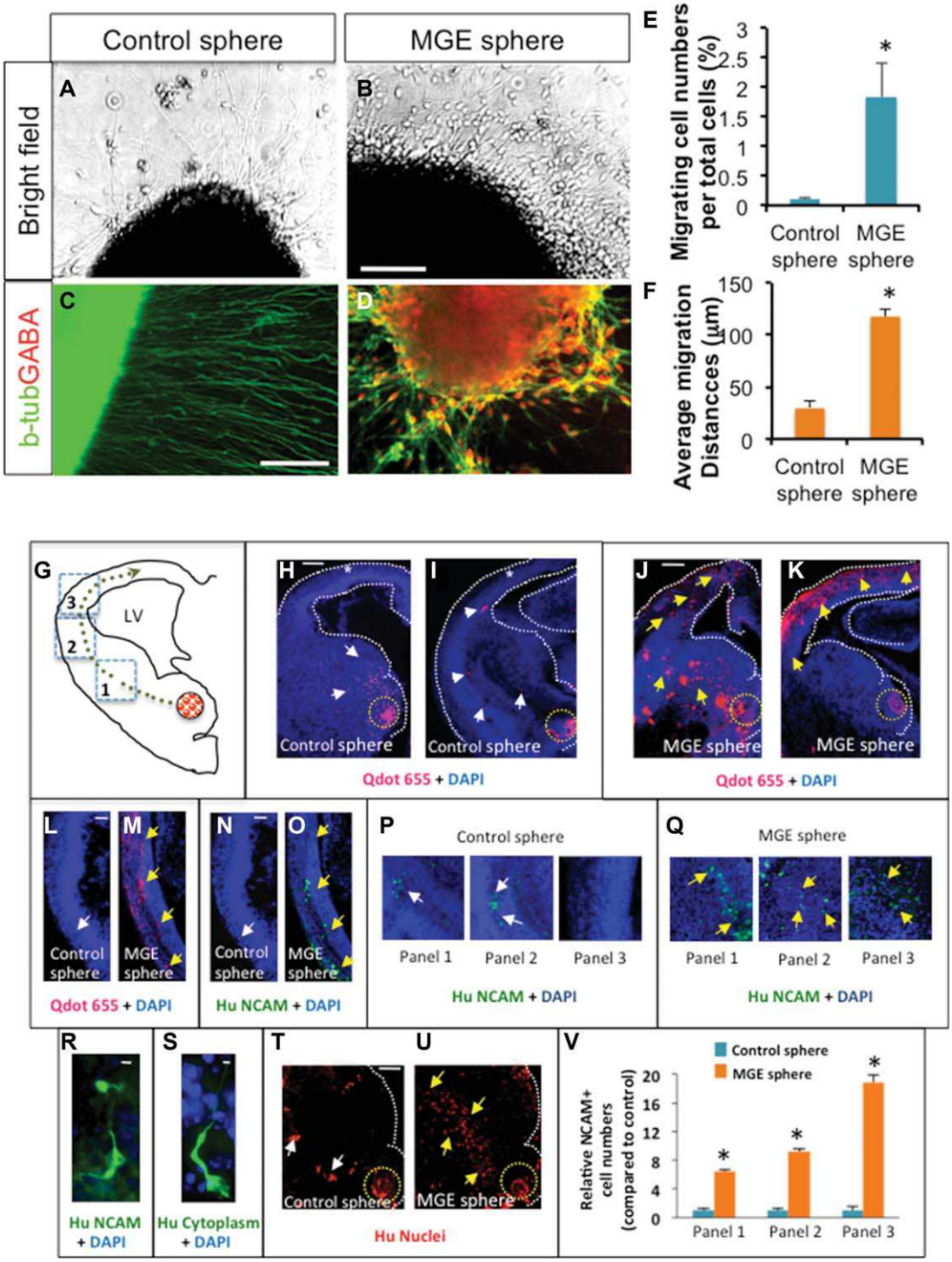

Figure 4.

during CNS development [33], we tested such possibility in our system. Exogenous application of FGF8 did increase FGF19 expression mildly but significantly, whereas exogenous application of FGF19 had no effect on FGF8 expression (Supporting Information Fig. S2H, S2I).

Generated CGE cells express another CGE marker Sp8 (Supporting Information Fig. S3A; 61.76% ± 7.86% $Sp8^+$/total cells, $n = 4$). $CoupTFII^+$ cells seldom coexpress Nkx2.1 (Supporting Information Fig. S3B) further supporting their CGE identity rather than dorsolateral or caudal MGE nor coexpress diencephalic marker Nkx2.2 (Supporting Information Fig. S3C). After further differentiation, these CoupTFII-expressing cells generated Vasoactive intestinal peptide (VIP)-expressing or Calretinin-expressing neurons (Supporting Information Fig. S3D, S3F; 10.46% ± 1.35% VIP^+/total cells and 16.77% ± 5.36% $Calretinin^+$/total cells, $n = 4$), consistent with their CGE identity [1], whereas only a few striatal projection neurons and no Somatostatin-expressing nor Parvalbumin-expressing neurons were present (Supporting Information Fig. S3H–S3K; 1.42% ± 0.49% $Isl1^+$/total cells and 1.06% ± 0.54% $Darpp32^+$/total cells, $n = 4$).

Optimized Induction Conditions Efficiently Generate MGE Cells from Multiple hPSCs

Thus, our optimized conditions use blocking Wnt signaling in the first and second week of differentiation, strong activation of the SHH pathway for the first 3 weeks of differentiation and FGF8 signaling in the second and third week of differentiation (Fig. 2A). Real-time PCR analysis under these optimal conditions showed that pluripotent stem cell markers Nanog and Oct4 expression is downregulated by day 3, and expression of ventral telencephalic markers Nkx2.1, GSX2, and DLX2 become evident starting at day 14, followed by expression of the postmitotic MGE marker Lhx6 at day 21 (Fig. 2B). We differentiated two human ESC (hESC) lines (H7 and H9) and one induced pluripotent stem cell (iPSC) line (iPSC2497) using MGE-inducing signals, and observed efficient MGE derivation ($Nkx2.1^+$) at day 25 of differentiation, whereas in absence of MGE-inducing signals (IWP2, SAG, and FGF8) all cells were of the dorsal telencephalic fate ($Pax6^+$) (Fig. 2C–2H). FACS analysis revealed that more than 80% of the total cells was induced to the MGE phenotype (Fig. 2I). Further immunocytochemistry analysis (Fig. 2J–2M) revealed that the majority of induced cells also express independent MGE markers Olig2 (71.8% ± 3.7% of total cells, $n = 4$) and FoxG1 (89.8% ± 2.0% of total cells, $n = 4$).

Human MGE Cells Generate GABAergic Interneurons

Further differentiation of MGE cells efficiently generated GABAergic neurons, based on Glutamic acid decarboxylase (GAD) expression (Fig. 3D–3F, 3G; 69.1% ± 4.1% GAD^+/total cells with 86.3% ± 4.0% β-$tubulin^+$/total cells), whereas without this treatment, few GAD-expressing neurons were observed (Fig. 3A–3G). In fact, absence of MGE inducing signaling yielded mostly glutamatergic neurons after differentiation (Supporting Information Fig. S4A, S4B), as expected from their $Pax6^+$ dorsal telencephalic identity. Robust induction of GABAergic neurons was also observed from H7- and iPSC2497-derived neurons under our optimized conditions (Fig. 3H, 3I; 88.8% ± 2.1% vs. 84.4% ± 3.4% $GABA^+/\beta$-$tubulin^+$ cells. $p = .32$, $n = 4$). These GABAergic neurons express Lhx6, showing their MGE origin; however, under control conditions, no Lhx6-expressing cells were observed (Fig. 3J–3P). H7 and iPSC2497 cells also robustly generated $Lhx6^+$ neurons under MGE-generating conditions (Fig. 3Q, 3R; 77.6% ± 4.5% vs. 74.4% ± 3.0% $Lhx6^+/\beta$-$tubulin^+$ cells. $p = .56$, $n = 4$). In addition, these GABAergic neurons coexpress Sox6 (Fig. 3S; 88.2% ± 2.5% $Sox6^+/GABA^+$ cells. $n = 4$), that was recently shown to be very specific marker for human MGE-derived interneurons [34]. Some of these cells expressed Calbindin (22.23% ± 6.0% total cells, $n = 4$; Fig. 3T), which is expressed in some of the migrating interneurons. Some of these cells express more mature interneuron markers Parvalbumin (0.87% ± 0.32% of total cells, $n = 4$; Fig. 3U–3W) and Somatostatin (1.53% ± 0.57% of total cells, $n = 4$; Fig. 3X–3Z) at this time point, as would be predicted from their MGE origin. We also observed the presence of minority of cells with alternate phenotypes at this time point (Supporting Information Fig. S4C–S4H; 0.86% ± 0.38% $Nkx2.2^+$/total cells, 1.24% ± 0.47% $isl1^+$/total cells, 0.32% ± 0.16% $ER81^+$/total cells, 0.63% ± 0.36% $ChAT^+$/total cells, 2.75% ± 1.05% $Tbr1^+$/total cells, $n = 4$). No midbrain dopaminergic neurons are

Figure 4. Migration property of human MGE cells. **(A–D):** MGE or cortical spheres derived from H9 human embryonic stem cells were plated on Matrigel substrate and analyzed 5 days after plating by bright field microscopy or immunocytochemistry. Scale bar = 100 μm. **(E):** Quantification of migrating cell numbers per sphere after 5 days in culture on Matrigel. Migrating cell numbers were normalized to total cell numbers in the sphere (mean ± SEM; $n = 3$, $p < .05$, two-tailed t test). **(F):** ImageJ software was used to assess each cell migration distance between the edge of the sphere and the center of the migrating cell body (mean ± SEM; $n = 3$, $p < .05$, two-tailed t test). **(G):** Schematic of transplantation of control and MGE spheres (red dotted circle) into the ventral telencephalon. Green dotted line points to route of migration of cells that emanated from the spheres. Dotted squares outline panels/areas in which the numbers of migrating cells were quantified. **(H–K):** Low magnification images (×4.2) of control and MGE sphere transplantations into E13.5 CD1 telencephalon. Yellow dotted circle indicates site of transplantation. Many cells were located close to the site of control sphere transplantation (white arrows, H) and few cells were observed migrating from ventral to dorsal telencephalon (white arrows, I). White stars (H, I) highlight decreased cell migration into dorsal telencephalon. In MGE sphere transplantation, many QDot-labeled cells migrated into the dorsal telencephalon (yellow arrows, J, K). White dotted lines (H–K) outline telencephalic boundaries. **(L–O):** Images (×10) of the dorsal telencephalon showing cells labeled with QDot nanocrystals (L, M) and anti-NCAM (N, O). White arrows point to decreased QDot (L) and NCAM label (N) and yellow arrows point to many QDot (M) and NCAM (O) labeled cells in the dorsal telencephalon. **(P, Q):** Migration of NCAM-labeled control (P) and MGE (Q) cells in three panels of the telencephalon as illustrated in the schema (G). White arrows (P) point to fewer cells and yellow arrows (Q) point to significant number of migrating cells. **(R):** High magnification image (×30) of migrating cells labeled with human NCAM antibody. **(S):** High magnification images (×60) of migrating cells labeled with human cytoplasm antibody. **(T–U):** Fewer human nuclei-positive cells migrated out from control sphere transplantations (white arrows, T) when compared with MGE sphere transplantations (yellow arrows, U). **(V):** Quantification of relative NCAM-positive cell numbers from cortical and MGE spheres in three panels of the telencephalon, after normalization using the average total cell numbers from parallel control and MGE spheres (*, $p < .001$, $n = 7$). Scale bars = H, 100 μm (applies also to I–K, T, U), L, 50 μm (applies M–O, P, Q), R, 25 μm, S, 10 μm. LV: lateral ventricle. Abbreviation: MGE, medial ganglionic eminence.

observed (Supporting Information Fig. S4I, S4J), consistent with our and other's previous study showing activation of Wnt signaling is important for specification of midbrain dopaminergic neurons [35, 36], whereas in the current protocol active inhibition of Wnt signaling was used. Very few VIP-expressing or Calretinin-expressing cells were observed at this time point

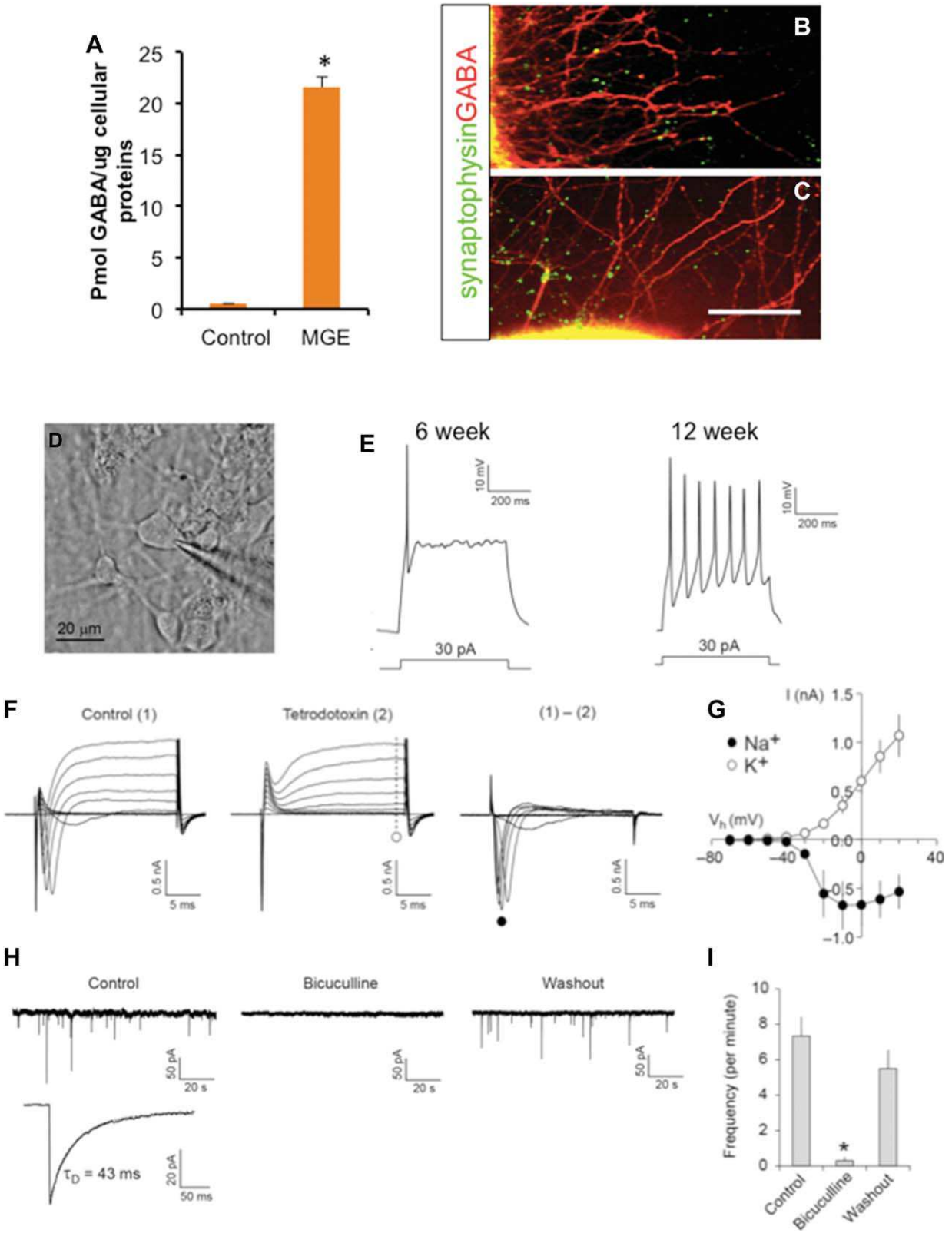

Figure 5.

(Supporting Information Fig. S3E, S3G). In addition, there were small number of olig2-expressing cells (2.86% ± 1.37% total cells, $n = 4$), but few mature astrocyte or oligodendrocyte differentiation observed at this time point (Supporting Information Fig. S4K–S4M), as expected from the long time it takes for human glia cells to mature [37–39].

During embryonic development, interneurons show robust tangential migration all the way to the developing cortex. We therefore tested whether hPSC-derived interneurons show such migratory characteristics. We reaggregated MGE-derived cells or uninduced control cells in low attach round-bottomed 96-well plates, and plated spheres on Matrigel-coated surfaces. Five days after plating, migration out of MGE cells clusters was observed compared to control clusters, and was expressed in terms of migrating cell numbers and migration distances (Fig. 4A–4F). Similar migration pattern was observed on matrigel-coated surfaces using mouse cortical versus MGE explant culture (Supporting Information Fig. S5A–S5D). In addition, when we embedded MGE explant and human MGE sphere in 3D matrigel matrixes, they also showed comparable migration pattern (Supporting Information Fig. S5E, S5F).

Heterochronic microtransplants were performed to test whether human MGE cells can migrate toward the cortex as in the case of in vivo development. Control and MGE spheres prelabeled with QDot nanocrystals were transplanted into the ventral telencephalon (MGE) of slices prepared from E13.5 CD1 embryos and cultured for 2 days. Slices were processed for paraffin histology and 20-μm-thick sections were used for immunohistochemistry and subsequent analysis. We binned the migration into three panels and performed a precise quantification of cell migration along the rostro-caudal axis in control and MGE sphere transplantations (Fig. 4G). Transplanted cells were detected by QDot fluorescence and additionally human NCAM, human nuclei, and human cytoplasm markers (Fig. 4H–4U). Cells that emanated from MGE spheres migrated robustly (Fig. 4J, 4K) and a significant number of cells that were QDot positive (Fig. 4J, 4K, 4M) and NCAM positive (Fig. 4O) were found in the dorsal telencephalon. In sharp contrast, cells from control spheres were found close to the transplantation site (Fig. 4H). QDot-positive (Fig. 4H, 4I, 4L) and NCAM-positive (Fig. 4N) cells were markedly reduced in the dorsal telencephalon in control sphere transplantations. Migratory cell morphology was detected with human NCAM and human cytoplasm antibodies at high magnifications (Fig. 4R, 4S). A human nucleus marker was used to further characterize identification and visualization of cell migration from transplanted control and MGE spheres (Fig. 4T, 4U). While fewer cells migrated from control spheres (Fig. 4T), robust cell migration was observed from MGE spheres (Fig. 4U), depicting robust migration in the ventral telencephalon en route to the dorsal telencephalon. Cell counting analysis of migrating NCAM+ cells showed significantly more MGE cells compared to control cells along the route of tangential migration from ventral to dorsal telencephalon (Fig. 4V).

HPLC analysis showed that generated interneurons produce robust GABA levels compared to control cells (Fig. 5A). One important functional characteristic of neurons is synapse formation to communicate with other neurons. Thus, we tested whether these MGE-derived neurons are able to form synaptic connections. Immunocytochemistry analysis followed by confocal microscopy showed that GABA-expressing neurites colocalized or juxtaposed with Synaptophysin foci, a presynaptic protein (Fig. 5B, 5C). Next, we examined whether MGE-derived cells have neuronal membrane properties using whole-cell patch-clamp technique (Fig. 5D). In current-clamp mode, injection of depolarizing currents to 6-week-old cells induced action potential firings in 4 out of 5 cells, whereas for 12-week-old cells all 10 cells examined fired action potential (Fig. 5E). Most 6-week-old cells displayed single action potentials, whereas 12-week-old cells started to show repetitive action potentials with uniform interspike intervals (1 out of 10 cells). Moreover, in voltage-clamp mode, voltage pulses evoked both transient inward currents and sustained outward currents, which were activated at membrane potential > -40 mV in all six cells examined (Fig. 5F, 5G). Rapidly desensitizing inward currents were completely blocked by tetrodotoxin, a voltage-gated Na^+ channel blocker, suggesting these cells express voltage-gated Na^+ channels. Next, we examined spontaneous postsynaptic currents to determine whether these cells form functional synapses. In voltage-clamp mode at −70 mV, spontaneous currents were detected in all 11 cells examined. These currents were blocked almost completely by bicuculline, a $GABA_A$ receptor inhibitor (Fig. 5H, 5I), indicating that the inhibitory neurotransmitter GABA mediated most of the spontaneous postsynaptic activities recorded in these cells. These results suggest that cells derived from hESCs form functional GABAergic synapses.

Figure 5. Functional properties of H9 MGE-derived GABAergic interneurons. **(A):** GABA determination from MGE-derived neuronal cultures by HPLC analysis (mean ± SEM; $n = 3$). **(B, C):** MGE-derived cells form synaptic connection, shown by overlap and juxtaposition of Synaptophysin foci with GABA staining after 6 weeks of differentiation. Scale bar = 100 μm. **(D):** A microscopic image of a recorded cell. **(E):** Representative traces of action potential firings induced by depolarizing current injection (500 ms long) in H9-derived MGE cells after 6 weeks and 12 weeks of differentiation. Injected currents are indicated. **(F):** Traces showing currents evoked by voltage pulses. Membrane potential was held at −70 mV in voltage-clamp mode. Left, square voltage pulses from −70 mV to 20 mV in increments of 10 mV (20 ms long) induced both transient inward and sustained outward currents (1). Middle, the application of tetrodotoxin (1 μM) selectively blocked transient component (2). Sustained outward currents insensitive to tetrodotoxin are likely mediated by voltage-gated K^+ channels (dotted line and open circle). Right, traces recorded under control conditions (1) were subtracted from currents recorded in the presence of tetrodotoxin (2) to calculate voltage-gated Na^+ currents at different membrane potentials (filled circle). **(G):** Current-voltage plots of voltage-dependent Na^+ and K^+ currents from traces as in F (filled and open circles, respectively; mean ± SEM; $n = 4$ cells). **(H):** Traces showing spontaneous postsynaptic currents. Left, spontaneous postsynaptic currents were recorded at −70 mV in voltage-clamp mode (upper trace). A lower trace is the average of spontaneous currents recorded in the same cell. Decay time constant (τ_D) was calculated by fitting the decay phase of the trace to a single exponential function (indicated by a dotted curve). Middle, the application of bicuculline (30 μM) blocked postsynaptic currents completely. Right, spontaneous postsynaptic currents were recovered fully after bicuculline washout. **(I):** Summary plot of H. Numbers of spontaneous postsynaptic currents were counted, and frequency per minute was calculated for each condition (mean ± SEM; $n = 4$ cells, *, $p < .05$, paired t test). Abbreviation: MGE, medial ganglionic eminence.

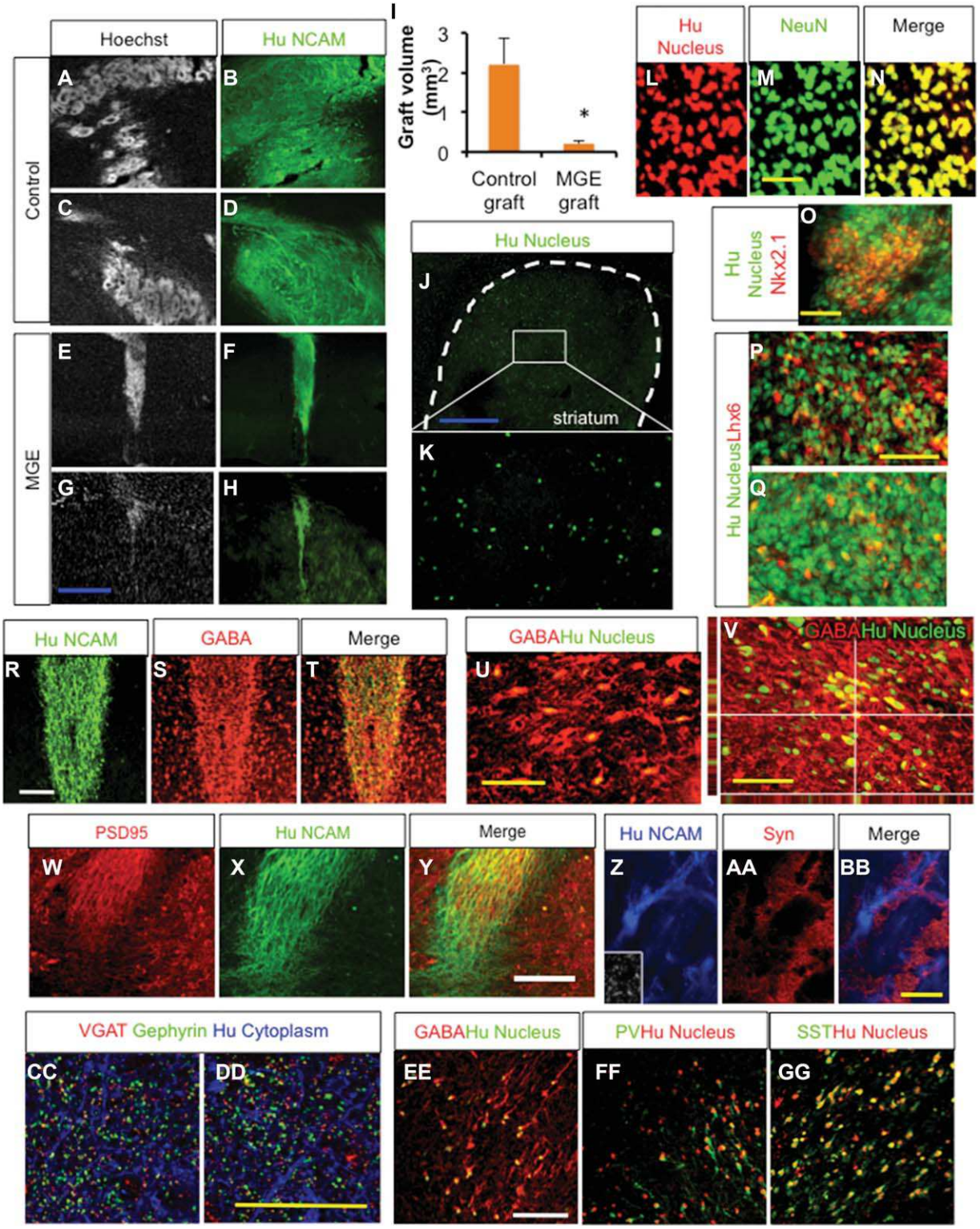

Figure 6. Transplanted MGE cells generate neural grafts enriched with GABAergic neurons. **(A–I):** H9-derived MGE cells generate well-contained neural grafts, whereas untreated cells (cortical cells) generate large and disruptive grafts with rosette structures, as analyzed 5 weeks after transplantation. (I) shows graft volume analysis of cortical cells versus MGE cells at this time point (mean ± SEM; $n = 10$, $p < .05$, two-tailed t test). **(J, K):** More grafted cells migrate in the host brain at 5 months after grafting. **(L–N):** MGE cells generated neural graft, shown by double staining of human nucleus-specific antibody with Neuronal Nuclei (NEUN) antibody, as analyzed 5 weeks postgrafting. **(O–Q):** Some of the grafted cells retain Nkx2.1 or Lhx6 expression at 5 weeks after transplantation. **(R–V):** MGE cells generate graft enriched with GABAergic neurons, as analyzed 5 weeks after transplantation. **(W–DD):** Immunocytochemistry analysis suggesting that MGE cells derived neurons form synaptic connection in the host brain. **(EE–GG):** Immunohistochemistry analysis 5 months postgrafting. Blue scale bar = 500 μm. White scale bar = 100 μm. Yellow scale bar = 50 μm. Abbreviation: MGE, medial ganglionic eminence.

Human MGE-Derived Cells Generate Well-Contained Neural Grafts Enriched with GABAergic Neurons

To analyze the in vivo behavior of human MGE-derived cells, we transplanted H9-derived interneurons at 5 weeks of differentiation into the striatum of NOD SCID mice. Control cells with dorsal telencephalic patterning were also transplanted for comparison. Whereas control cells massively proliferate and form big grafts with rosette structures (Fig. 6A–6D) reminiscing of their massive proliferation during human brain development, MGE-derived cells form well-contained grafts (Fig. 6E–6H). Supporting this observation, the average graft volume of cortical cells was 2.22 ± 0.64 mm^3, whereas that of MGE-derived cells was 0.21 ± 0.07 mm^3. Five weeks postgrafting, some cells were observed to have migrated out of the MGE graft core into the host brain, but, more cells migrated out of the graft core 5 months after grafting (Supporting Information Fig. S6A–S6C; $4{,}810 \pm 1{,}309$ cells per graft [$n = 10$] for 5-week grafts and $5{,}438 \pm 2{,}082$ cells per graft [$n = 5$] for 5 months grafts), sometimes with no graft core at all with even distribution of the grafted cells throughout the entire striatum (Fig. 6J, 6K). MGE-derived cells generated mostly neural grafts, shown by colabeling of human nucleus with NeuN (Fig. 6L–6N; $77.5\% \pm 7.0\%$ NeuN$^+$/Human Nuclei$^+$ cells) and β-tubulin (Supporting Information Fig. S6D–S6F). Some of the these cells retained Nkx2.1 expression (Fig. 6O; $27.57\% \pm 7.83\%$ Nkx2.1$^+$/Human Nuclei$^+$ cells) at 5 weeks post-transplantation, and some of them expressed the MGE-derived interneuron-specific transcription factor Lhx6 (Fig. 6P, 6Q; $22.53\% \pm 2.78\%$ Lhx6$^+$/Human Nuclei$^+$ cells), which is expressed in all MGE-derived migrating immature interneurons and subsequently is downregulated in some of mature MGE-derived interneurons [1]. Transplanted cells generated grafts largely composed of GABAergic interneurons, shown by coexpression of GABA with human NCAM and human nuclei (Fig. 6R–6V; $58.97\% \pm 4.52\%$ GABA$^+$/human Nuclei$^+$ cells). At 5 weeks postgrafting, there were small portion of immature proliferating cells present in the graft, which was further reduced by 5 months postgrafting (Supporting Information Fig. S6G, S6H; $5.59\% \pm 3.46\%$ and $1.05\% \pm 0.74\%$ Ki67$^+$/Human Nuclei$^+$ cells, respectively). There are minority of cells with alternate phenotypes as shown in Supporting Information Figure S6I–S6N ($0.69\% \pm 0.38\%$ Nkx2.2$^+$/Human Nuclei$^+$ cells, $4.48\% \pm 1.02\%$ CoupTFII$^+$/Human Nuclei$^+$ cells, $0.72\% \pm 0.31\%$ ER81$^+$/Human Nuclei$^+$ cells, $0.89\% \pm 0.52\%$ Darpp32$^+$/Human Nuclei$^+$ cells, $0.95\% \pm 0.33\%$ Tbr1$^+$/Human Nuclei$^+$ cells, and $1.05\% \pm 0.62\%$ ChAT$^+$/Human Nuclei$^+$ cells). There were few astrocytes or oligodendrocytes at this time point (Supporting Information Fig. S6O–S6P). PSD95 foci overlapped with human-specific NCAM$^+$ fibers (Fig. 6W–6Y), suggestive of glutamatergic synaptic connection from the host to the graft. Synaptic connection with the host brain was also indicated by colocalization or juxtaposition of human NCAM with Synaptophysin foci (Fig. 6Z–6BB). In the same line, many Vesicular GABA transporter (VGAT) foci were observed juxtaposed with Gephyrin foci (Fig. 6CC, 6DD), and Synaptophysin foci with PSD95 foci (Supporting Information Fig. S6Q). In addition, in 5-month-old grafts, parvalbumin-expressing or somatostatin-expressing neurons are often observed (Fig. 6EE–6GG; $15.7\% + 6.1\%$ Parvalbumin$^+$/Human Nuclei$^+$ cells and $17.7\% + 5.9\%$ Somatostatin$^+$/Human Nuclei$^+$ cells), confirming the developmental potential of generated MGE cells.

Discussion

Efficient generation of homogeneous populations of specific differentiated progenies of hPSCs is an important prerequisite to realize the full potential of hPSCs for disease modeling, regenerative medicine, and bioassays [12]. In this study, using a stepwise combined and temporal regulation of dorsolateral and rostrocaudal signaling pathways we achieved a very effective and homogeneous differentiation of hPSCs to MGE cells and then to GABAergic interneurons. Recent reports of efficient derivation of MGE cells showed conflicting results on the effect of timing of SHH activation, one study using early activation of SHH for efficient induction of MGE cells [17], but the other showing that only late activation of SHH resulted in efficient MGE induction with early SHH activation mainly resulting in no MGE induction [18], although both study used highly similar signaling modulation such as double SMAD inhibition (SB431542 along with BMP inhibitor Noggin or LDN193189), Wnt inhibition (DKK1), and strong SHH activation. In this study, we showed the pleiotropic effect of strong SHH signaling activation during early human neural differentiation, resulting in activation of mutually antagonizing signals. We also identified exogenous FGF8 addition as a way to overcome such pleiotropic and stochastic induction of MGE cell type by strong SHH activation and generated reliable populations of MGE cells, regardless of stochastic shift in SHH downstream signaling.

Salient features of our procedure include; first, a more efficient ventral telencephalic phenotype induction achieved by early modulation of Wnt and SHH signaling pathways even before neuroectoderm formation is completed, in line with the previous report [17]. This is consistent with previous developmental studies, where early inhibition of Wnt signaling is important for telencephalic induction of neural plate [27, 28] and early SHH signaling in anterior neural plate at the gastrula stage induces prospective ventral telencephalon, [40] even prior to neural tube formation. Maroof et al. also showed that early SHH activation is more effective in ventralization as illustrated by higher Nkx2.1 induction (>80% vs. approximately 50%; early vs. late SHH activation), [18] although they failed to fully derive MGE cells using early SHH activation and instead generated diencephalic cells. Second, the combined use of dorsoventral as well as rostrocaudal modulation using developmentally relevant signaling pathways resulted in accumulative increase of MGE induction, into very homogeneous populations. Here, we have used (a) induction of neuroectoderm formation by double-SMAD inhibition [25], (b) inhibition of Wnt signaling, which otherwise caudalize [27, 28] and dorsalize [29] differentiating neuroectoderms, (c) strong activation of SHH signaling, resulting in MGE induction at the expense of LGE induction with mild SHH signaling, and (d) activation of FGF8 signaling, which induces the MGE phenotype at the expense of the more caudal CGE phenotype. In a previous study [41], a method using Activin A was shown to induce CGE type cells from mouse and hPSCs, generating another important class of cortical interneurons. In this study, we provide an alternate method to generate human CGE cells that express CoupTFII as well as Sp8 using step-wise approach that recapitulates normal embryonic development. To our knowledge, this is the most efficient and massive generation of human CGE cells (up to 80% of total cells). Such combined and temporal activation was also observed during differentiation of

mouse ESCs [23], suggesting the conserved nature of early neural phenotype specification between these two species. In the absence of such signaling molecule modulation, most of the cells take up a dorsal telencephalic identity, in agreement with previous observation of human PSCs differentiation [5, 42].

In early brain development, FGF8 is expressed in the anterior neural ridge and is known to play an important role in determining rostral-caudal boundary whereby increased expression shifts the MGE and CGE boundary posteriorly [6]. SHH induces the ventral phenotype in the telencephalon by repressing Gli3 function [20], which represses FGF8 expression [21] and could indirectly induce FGF8 expression through repression of Gli3, indirectly exerting rostralizing activity. However, to complicate matters, it was also shown that SHH induces FGF15/19 expression in the forebrain development [22, 24], which was shown to antagonize the function of FGF8 during ventral telencephalic development [22, 23]. These developmental studies imply that small stochastic shift in SHH downstream signaling result in drastic shift of generated differentiation progenies, and demonstrate the power of developmental knowledge to reliably direct specific neural subtype differentiation.

MGE-derived interneurons show the ability to spontaneously differentiate into Lhx6-expressing GABAergic interneurons, showing them as phenotype-specified neural progenitors with intrinsic properties to become GABAergic interneurons. Enriched expression of Lhx6 after differentiation further demonstrates the MGE characteristic of derived progenitors, since Lhx6 expression is not observed in the preoptic area in the ventral telencephalon where Nkx2.1 is also expressed [43] nor in CGE-derived interneurons [1]. Derivation of a homogeneous MGE population was further confirmed by the limited presence of CoupTFII-expressing cells as well as the paucity of Pax6-expressing progenitors. The migratory property observed by these hPSC-derived interneurons on matrigel substrate and on E13.5 telencephalic slices well recapitulates their in vivo counterparts (Supporting Information Fig. S5A–S5E and [44–46]). Remarkably, human MGE-derived neurons displayed physiological and electrophysiological properties consistent with GABAergic interneurons such as their ability to produce GABA, formation of synaptic connection, and generation of action potentials and GABAergic postsynaptic activity. Even though postmitotic neuronal markers such as GAD and β-tubulin were robustly expressed at 6 weeks of differentiation, not all cells at this stage were able to fire action potentials, while at 12 weeks of differentiation all cells tested were able to. This long-term maturation process has been reported before [17, 47], and is likely to reflect the long-term maturation process of human brain development. The small proportions of MGE-derived interneurons that mature to express somatostatin and parvalbumin at 6 weeks of differentiation are also in line with this notion of long-term maturation of human neurons. Such early developing interneurons before full maturation will be of great value for cell replacement therapy with its migratory functions and for modeling neurodevelopmental disease such as schizophrenia enabling us to model early developmental time point during which the developing brains are known to be more susceptible to environmental challenge [48–50], and many known schizophrenia risk genes are highly expressed [51–53].

Another significant finding of this study is that hPSC-derived interneurons not only generated well-integrated grafts with migratory properties. This is in contrast with transplantation of control cells without MGE inducing signals, which extensively proliferated and generated large grafts with rosette structures in the striatum, reminiscent of their massive proliferation during human dorsal telencephalic development. Furthermore, we found that hPSC-derived MGE grafts were enriched with GABAergic interneurons, that mature to express somatostatin and parvalbumin. Recent studies have shown the potential of GABAergic interneurons as sources for novel cellular therapies for epilepsy [54], Parkinson's disease [46], and injury-induced neuropathic pain [55]. Considering that optimal cell sources for such therapy are limiting, the development of a homogeneous population of human GABAergic interneurons brings this novel therapy one step closer to the clinic. For translational studies as a next step, more experiments with longer term grafting in many more mice would be needed to rule out the possibility of tumor formation and to further assure the safety of the human cell grafts.

Conclusions

In summary, functional and authentic human MGE cells and GABAergic interneurons recapitulating the in vivo ventral telencephalic development can be efficiently generated in vitro by developmentally relevant dorsoventral and rostrocaudal modulation. This novel strategy will be useful in regenerative medicine, developmental studies, disease modeling, bioassay, and drug screening.

Acknowledgments

We thank Dr. Pachnis for kindly providing us with anti-Lhx6 antibodies. This study was supported by NIH grants (NS079977, MH048866, MH087903, and NS070577) and Harvard Stem Cell Institute Seed Grant.

Author Contributions

T.-G.K.: conception and design, collection and assembly of data, and data analysis and interpretation; R.Y., A.K., and T.M.: collection and assembly of data and data analysis and interpretation; J.-H.C. and A.V.: conception and design, collection and assembly of data, data analysis and interpretation, and manuscript writing; P.K.T., M.M., D.D.: collection and assembly of data; V.Y.B.: conception and design and data analysis and interpretation; K.-S.K.: financial support and manuscript writing; S.C.: conception and design, financial support, collection and assembly of data, data analysis and interpretation, and manuscript writing.

Disclosure of Potential Conflicts of Interest

The authors indicate no potential conflicts of interest.

References

1 Wonders CP, Anderson SA. The origin and specification of cortical interneurons. Nat Rev Neurosci 2006;7:687–696.
2 Tamamaki N, Yanagawa Y, Tomioka R et al. Green fluorescent protein expression and colocalization with calretinin, parvalbumin, and somatostatin in the GAD67-GFP knock-in mouse. J Comp Neurol 2003;467: 60–79.
3 Chiang C, Litingtung Y, Lee E et al. Cyclopia and defective axial patterning in mice lacking Sonic hedgehog gene function. Nature 1996;383:407–413.
4 Fuccillo M, Rallu M, McMahon AP et al. Temporal requirement for hedgehog signaling in ventral telencephalic patterning. Development 2004;131:5031–5040.
5 Li XJ, Zhang X, Johnson MA et al. Coordination of sonic hedgehog and Wnt signaling determines ventral and dorsal telencephalic neuron types from human embryonic stem cells. Development 2009; 136:4055–4063.
6 Fukuchi-Shimogori T, Grove EA. Neocortex patterning by the secreted signaling molecule FGF8. Science 2001;294:1071–1074.
7 Garel S, Huffman KJ, Rubenstein JL. Molecular regionalization of the neocortex is disrupted in Fgf8 hypomorphic mutants. Development 2003;130:1903–1914.
8 Sussel L, Marin O, Kimura S et al. Loss of Nkx2.1 homeobox gene function results in a ventral to dorsal molecular respecification within the basal telencephalon: Evidence for a transformation of the pallidum into the striatum. Development 1999;126:3359–3370.
9 Liodis P, Denaxa M, Grigoriou M et al. Lhx6 activity is required for the normal migration and specification of cortical interneuron subtypes. J Neurosci 2007;27:3078–3089.
10 Arber CE, Li M. Cortical interneurons from human pluripotent stem cells: Prospects for neurological and psychiatric disease. Front Cell Neurosci 2013;7.
11 Castiglioni V, Onorati M, Rochon C et al. Induced pluripotent stem cell lines from Huntington's disease mice undergo neuronal differentiation while showing alterations in the lysosomal pathway. Neurobiol Dis 2012;46: 30–40.
12 Bellin M, Marchetto MC, Gage FH et al. Induced pluripotent stem cells: The new patient? Nat Rev Mol Cell Biol 2012;13:713–726.
13 Matsui T, Akamatsu W, Nakamura M et al. Regeneration of the damaged central nervous system through reprogramming technology: Basic concepts and potential application for cell replacement therapy. Exp Neurol 2012.
14 Brennand KJ, Simone A, Jou J et al. Modelling schizophrenia using human induced pluripotent stem cells. Nature 2011; 473:221–225.
15 Lee G, Ramirez CN, Kim H et al. Large-scale screening using familial dysautonomia induced pluripotent stem cells identifies compounds that rescue IKBKAP expression. Nat Biotechnol 2012;30:1244–1248.
16 Egawa N, Kitaoka S, Tsukita K et al. Drug screening for ALS using patient-specific induced pluripotent stem cells. Sci Transl Med 2012;4:145ra104.
17 Nicholas CR, Chen J, Tang Y et al. Functional maturation of hPSC-derived forebrain interneurons requires an extended timeline and mimics human neural development. Cell Stem Cell 2013;12:573–586.
18 Maroof AM, Keros S, Tyson JA et al. Directed differentiation and functional maturation of cortical interneurons from human embryonic stem cells. Cell Stem Cell 2013;12: 559–572.
19 Liu Y, Weick JP, Liu H et al. Medial ganglionic eminence-like cells derived from human embryonic stem cells correct learning and memory deficits. Nat Biotechnol 2013; 31:440–447.
20 Rallu M, Machold R, Gaiano N et al. Dorsoventral patterning is established in the telencephalon of mutants lacking both Gli3 and Hedgehog signaling. Development 2002; 129:4963–4974.
21 Aoto K, Nishimura T, Eto K et al. Mouse GLI3 regulates Fgf8 expression and apoptosis in the developing neural tube, face, and limb bud. Dev Biol 2002;251:320–332.
22 Borello U, Cobos I, Long JE et al. FGF15 promotes neurogenesis and opposes FGF8 function during neocortical development. Neural Dev 2008;3:17.
23 Danjo T, Eiraku M, Muguruma K et al. Subregional specification of embryonic stem cell-derived ventral telencephalic tissues by timed and combinatory treatment with extrinsic signals. J Neurosci 2011;31:1919–1933.
24 Ishibashi M, McMahon AP. A sonic hedgehog-dependent signaling relay regulates growth of diencephalic and mesencephalic primordia in the early mouse embryo. Development 2002;129:4807–4819.
25 Chambers SM, Fasano CA, Papapetrou EP et al. Highly efficient neural conversion of human ES and iPS cells by dual inhibition of SMAD signaling. Nat Biotechnol 2009;27: 275–280.
26 Chung S, Moon J-I, Leung A et al. ES cell-derived renewable and functional midbrain dopaminergic progenitors. Proc Natl Acad Sci USA 2011;108:9703–9708.
27 Houart C, Caneparo L, Heisenberg C et al. Establishment of the telencephalon during gastrulation by local antagonism of Wnt signaling. Neuron 2002;35:255–265.
28 Nordstrom U, Jessell TM, Edlund T. Progressive induction of caudal neural character by graded Wnt signaling. Nat Neurosci 2002; 5:525–532.
29 Gunhaga L, Marklund M, Sjodal M et al. Specification of dorsal telencephalic character by sequential Wnt and FGF signaling. Nat Neurosci 2003;6:701–707.
30 Gulacsi A, Anderson SA. Shh maintains Nkx2.1 in the MGE by a Gli3-independent mechanism. Cereb Cortex 2006;(16 suppl 1): i89–95.
31 Hebert JM, Fishell G. The genetics of early telencephalon patterning: Some assembly required. Nat Rev Neurosci 2008;9:678–685.
32 Ruiz i Altaba A, Palma V, Dahmane N. Hedgehog-Gli signalling and the growth of the brain. Nat Rev Neurosci 2002;3:24–33.
33 Gimeno L, Martinez S. Expression of chick Fgf19 and mouse Fgf15 orthologs is regulated in the developing brain by Fgf8 and Shh. Dev Dyn 2007;236:2285–2297.
34 Ma T, Wang C, Wang L et al. Subcortical origins of human and monkey neocortical interneurons. Nat Neurosci 2013;16:1588–1597.
35 Chung S, Leung A, Han BS et al. Wnt1-lmx1a forms a novel autoregulatory loop and controls midbrain dopaminergic differentiation synergistically with the SHH-FoxA2 pathway. Cell Stem Cell 2009;5:646–658.
36 Kriks S, Shim JW, Piao J et al. Dopamine neurons derived from human ES cells efficiently engraft in animal models of Parkinson's disease. Nature 2011;480:547–551.
37 Krencik R, Weick JP, Liu Y et al. Specification of transplantable astroglial subtypes from human pluripotent stem cells. Nat Biotechnol 2011;29:528–534.
38 Wang S, Bates J, Li X et al. Human iPSC-derived oligodendrocyte progenitor cells can myelinate and rescue a mouse model of congenital hypomyelination. Cell Stem Cell 2013; 12:252–264.
39 Hu BY, Du ZW, Zhang SC. Differentiation of human oligodendrocytes from pluripotent stem cells. Nat Protoc 2009;4:1614–1622.
40 Gunhaga L, Jessell TM, Edlund T. Sonic hedgehog signaling at gastrula stages specifies ventral telencephalic cells in the chick embryo. Development 2000;127:3283–3293.
41 Cambray S, Arber C, Little G et al. Activin induces cortical interneuron identity and differentiation in embryonic stem cell-derived telencephalic neural precursors. Nat Commun 2012;3:841.
42 Mariani J, Simonini MV, Palejev D et al. Modeling human cortical development in vitro using induced pluripotent stem cells. Proc Natl Acad Sci USA 2012;109:12770–12775.
43 Flames N, Pla R, Gelman DM et al. Delineation of multiple subpallial progenitor domains by the combinatorial expression of transcriptional codes. J Neurosci 2007;27: 9682–9695.
44 Wichterle H, Garcia-Verdugo JM, Herrera DG et al. Young neurons from medial ganglionic eminence disperse in adult and embryonic brain. Nat Neurosci 1999;2:461–466.
45 Alvarez-Dolado M, Calcagnotto ME, Karkar KM et al. Cortical inhibition modified by embryonic neural precursors grafted into the postnatal brain. J Neurosci 2006;26: 7380–7389.
46 Martinez-Cerdeno V, Noctor SC, Espinosa A et al. Embryonic MGE precursor cells grafted into adult rat striatum integrate and ameliorate motor symptoms in 6-OHDA-lesioned rats. Cell Stem Cell 2010;6:238–250.
47 Johnson MA, Weick JP, Pearce RA et al. Functional neural development from human embryonic stem cells: Accelerated synaptic activity via astrocyte coculture. J Neurosci 2007;27:3069–3077.
48 Aguilar-Valles A, Luheshi GN. Alterations in cognitive function and behavioral response to amphetamine induced by prenatal inflammation are dependent on the stage of pregnancy. Psychoneuroendocrinology 2011;36: 634–648.
49 Piper M, Beneyto M, Burne TH et al. The neurodevelopmental hypothesis of schiz-

ophrenia: Convergent clues from epidemiology and neuropathology. Psychiatr Clin North Am 2012;35:571–584.
50 Li Q, Cheung C, Wei R et al. Prenatal immune challenge is an environmental risk factor for brain and behavior change relevant to schizophrenia: Evidence from MRI in a mouse model. PLoS One 2009;4: e6354.
51 Xu B, Ionita-Laza I, Roos JL et al. De novo gene mutations highlight patterns of genetic and neural complexity in schizophrenia. Nat Genet 2012;44:1365–1369.
52 Lin M, Pedrosa E, Shah A et al. RNA-Seq of human neurons derived from iPS cells reveals candidate long non-coding RNAs involved in neurogenesis and neuropsychiatric disorders. PLoS One 2011;6:e23356.
53 Gilman SR, Chang J, Xu B et al. Diverse types of genetic variation converge on functional gene networks involved in schizophrenia. Nat Neurosci 2012;15:1723–1728.
54 Baraban SC, Southwell DG, Estrada RC et al. Reduction of seizures by transplantation of cortical GABAergic interneuron precursors into Kv1.1 mutant mice. Proc Natl Acad Sci USA 2009;106: 15472–15477.
55 Braz JM, Sharif-Naeini R, Vogt D et al. Forebrain GABAergic neuron precursors integrate into adult spinal cord and reduce injury-induced neuropathic pain. Neuron 2012;74:663–675.


See www.StemCells.com for supporting information available online.